Supporting Information

Electrocatalytic Activity of 1D/3D TiO_2 Tubular Layers/Ni-Modified MXene Microsphere Heterojunction Electrodes

Dujearic-Stephane Kouao [a]*, Agnieszka Kramek [b], Justyna Gumieniak [b], Karol Załęski [c], Emerson Coy [c], Jakub Karczewski [d], Guowei Li [e,f], Katarzyna Siuzdak [a]*

[a] *Centre for Plasma and Laser Engineering, Institute of Fluid-Flow Machinery, Polish Academy of Sciences, 14 Fiszera St., 80-231 Gdańsk, Poland.*
[b] *The Faculty of Mechanics and Technology, Rzeszów University of Technology, Kwiatkowskiego 4 St., 37-450 Stalowa Wola, Poland .*
[c] *NanoBioMedical Centre, Adam Mickiewicz University, Wszechnicy Piastowskiej 3 St., 61-614 Poznań, Poland.*
[d] *Faculty of Applied Physics and Mathematics, Institute of Nanotechnology and Materials Engineering, Gdańsk University of Technology, Narutowicza 11/12 St,, 80-233 Gdańsk, Poland.*
[e] *Zhejiang Provincial Key Laboratory of Magnetic Materials and Applications, Ningbo Institute of Materials Technology and Engineering, Chinese Academy of Sciences, Ningbo 315201, China.*
[f] *Center of Materials Science and Optoelectronics Engineering, University of Chinese Academy of Sciences, 19 A Yuquan Rd, Shijingshan District, Beijing 100049, China.*

**Corresponding authors.*
E-mail addresses: dkouao@imp.gda.pl, ksiuzdak@imp.gda.pl

1. Experimental section

1.1. Materials and reagents

Tetrafluoroboric acid (HBF_4, 500 mL, 48 wt% in H_2O, Sigma-Aldrich), Tetramethylammonium tetrafluoroborate (TMATBF, 99%, AmBeed), cellulose acetate (Sigma-Aldrich), acetone (99.7 %, Protolab), ammonium fluoride (99.7 %, Chempur), sodium hydroxide (98.8 %, Chempur), diethylene glycol (99.6 %, Chempur), Ti_3AlC_2 MAX powder (> 99 %, 325 mesh, Nanografi), titanium foil (99.7% pure, 0.127 mm thick, Strem), nickel chloride hexahydrate (99.9 %, Sigma-Aldrich), iridium oxide coated Ti electrode (Laborxing), 20% platinum on carbon electrode (Fuel cell store).

1.2. Electrochemical etching of Ti_3AlC_2 MAX phase

TMATBF (0.5 g) was dissolved in DMSO (10 mL) by ultrabath sonication for 10 min in a plastic beaker. Then, HBF_4 (10 mL) was added to the mixture, and the resultant solution was sonicated for another 10 min. This solution was poured into the electrochemical cell containing

a thermostatically controlled jacket to maintain the cell temperature at 65 °C. For safety issue, we recommend using electrochemical cells made of acid-resistant plastic, i.e. PEEK, for this experiment. Ti_3AlC_2 powder (150 mg) was added under constant stirring of the suspension (300 rpm). The etching of Ti_3AlC_2 was performed in a three-electrode system using Ag/AgCl/0.1 M KCl as the reference electrode and two square glassy carbon electrodes (25 × 25 mm^2) spaced 20 mm apart, one serving as the working electrode and the other as the counter electrode. Then, cyclic voltammetry (CV) was carried out within the potential range of –1 to +1 at 20 mVs^{-1}. The number of cycles varied from 100 to 300. When the electrochemical process reached established number of cycles, the suspension was taken out of the electrochemical cell and sonicated for 2h. Afterwards, the post-reaction suspension was centrifuged at 6000 rpm (MPW-251, MPW Med. Instruments) for 4 min, and the material collected at the bottom was dispersed in deionized water. This procedure was repeated five times to remove impurities. The sediment at the bottom was dried overnight in a vacuum desiccator to obtain a powder. Depending on the number of cycles applied during electrochemical process, prepared materials were labelled as MX-100, MX-200 and MX-300 when 100, 200 and 300 CV curves were recorded. The scheme of the electrochemical cell is presented in **Figure S1**, and the flowchart of the synthesis process with optimized process parameters is also provided in the supplementary file (**Figure S2**). For comparison, MXene was also prepared by the tradition traditional HF-etching method described in our previous work and was labelled as MX-HF [1].

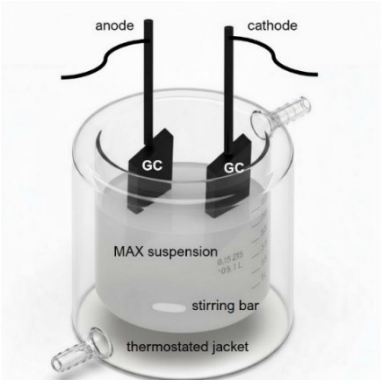

Figure S1. Schematic illustration of the electrochemical setup used for the MXenes electrochemical synthesis using MAX phase containing suspension.

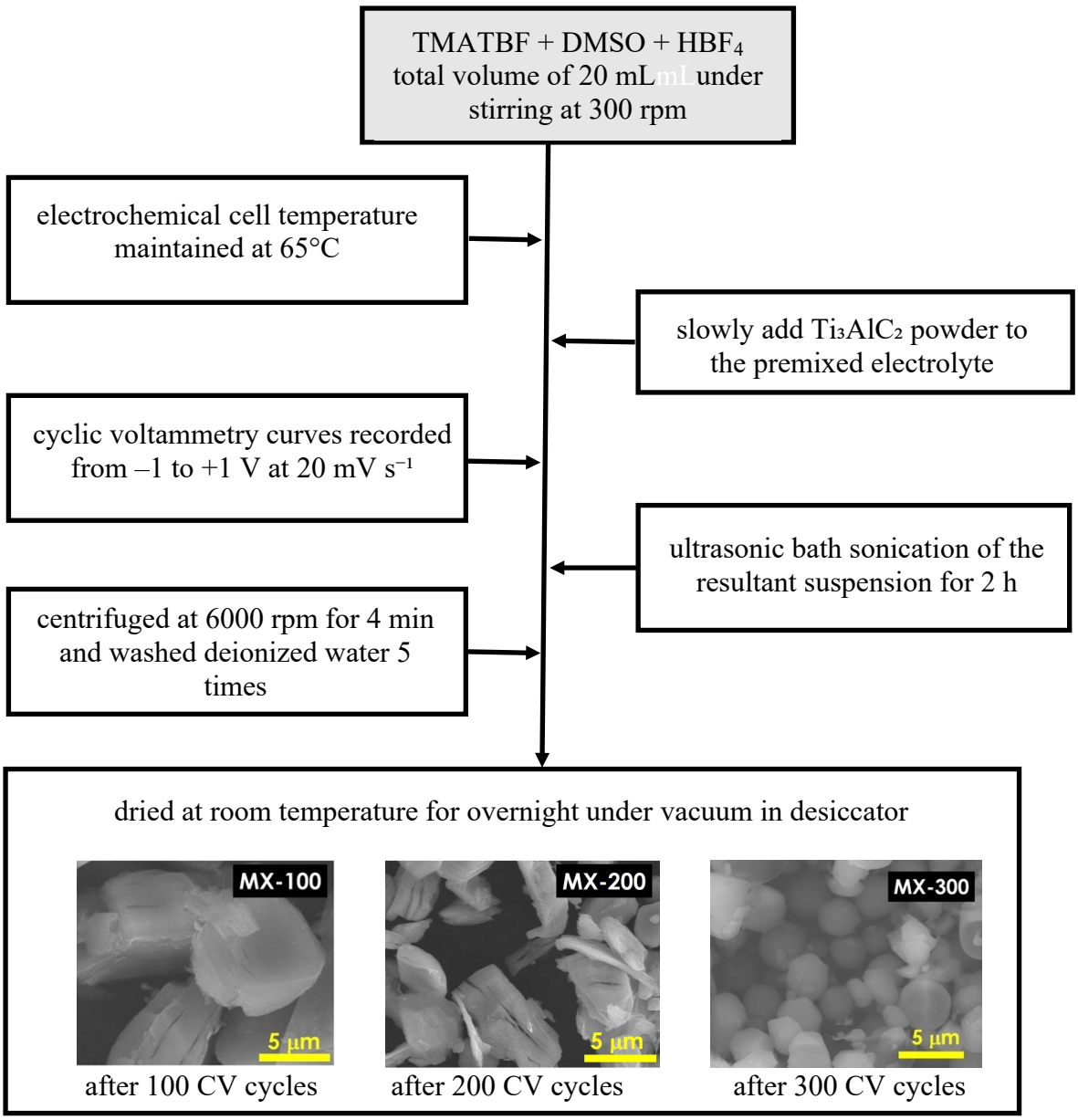

Figure S2. The flowchart of the synthesis process including electrochemical etching stage.

1.3. Modification of MXene with Ni

Nickel chloride hexahydrate (2.3 g) was dissolved in deionized water (10 mL) and this process was supported by 30 min stirring (300 rpm) [2]. Then, the MXene (0.1 g) obtained after 300 CV cycles of etching (MX-300) and fabricated using traditional method (MX-HF) was added into the nickel salt solution. The selection of MX-300 for this modification was based on the morphology as will be discussed in the section concerning morphology inspection. The resulting mixture was stirred (200 rpm) at room temperature for 24 h and then centrifuged at 6000 rpm for 4 min. The collected material was dried overnight. Due to the nickel modification,

additional two materials were produced NiMX-300 and NiMX-HF, to show the impact of the fabrication method onto the electrochemical activity towards water splitting.

1.4. Fabrication of titania nanotubes (TN) materials

The titanium foil was cut into rectangular shape (30 × 20 mm^2) and then cleaned successively in the following order: acetone, ethanol and deionized water in an ultrasonic bath for 10 min in each medium. After air drying, the foil was immersed in an electrolyte consisting of a mixture of diethylene glycol (93 vol%) and deionized water (7 vol%), containing ammonium fluoride (0.15 M) and hydrofluoric acid (0.5 M). The temperature of the electrochemical cell was maintained at 40 °C, and a voltage of 60 V was applied between the Ti foil serving as an anode and a platinum mesh acting as a cathode for 2h. After anodization the foils were washed gently by ethanol and deionized water. The fabricated layer is composed of laterally spaced nanotubes with an average tube length, external diameter and wall thickness of 2.5 ± 0.4 μm, 320 ± 16 nm and 50 ± 8 nm, respectively. More details on the dependence of the morphological characteristics of nanotubes on anodizing conditions is described in details in our previous work [3].

1.5. Fabrication of a hierarchical NiMX-300@TN heterojunction catalyst

The binder solvent was first prepared by dissolving cellulose acetate (5 mg) into acetone (1 mL) by magnetic stirring for 15 min. Then, nickel modified MXene (0.1 g), i.e., NiMX-300 (or NiMX-HF) and the binder solution (300 μL) were mixed in a mortar to obtained a gel-like slurry. The resulting suspension (25 μL) was dropped onto the TiO_2 tubular layer. Then, the sample was subjected to rapid heat treatment for 1 min at a heating rate of 0.67 °C/s in air i.e., a-NiMX-300@TN (or a-NiMX-HF@TN) or under a hydrogen atmosphere i.e., h-NiMX-300@TN (or h-NiMX-HF@TN), in order to perform crystallisation of the titania nanotubes and improve their electrochemical properties.[4] The resultant material obtained after the thermal treatment was directly used as the working electrode for the electrochemical testing.

1.6. Characterization methods

Scanning electron microscope (SEM) images were captured using Hitachi SU3500. Transmission electron microscope (TEM) pictures were done using (ARM 200F, JEOL) 200 eV equipped with an energy-dispersive X-ray spectrometer (EDX). Raman measurements were performed using a Raman spectrometer (Renishaw) equipped with a 785 nm red diode laser and operating at 1 % of its total power. The spectra were recorded in the wave number range from 100 to 2000 cm^{-1} using the objective 20×. The chemical structure of the samples was measured by X-ray photoelectron spectroscopy using a Thermo Scientific™ K-Alpha™ X-ray photoelectron spectrometer (XPS). The samples were irradiated with Al Kα = 1486.7 eV X-ray

radiation. Measurements were carried out under a pressure of 10^{-9} to 10^{-8} mbar. Survey spectra were registered using a pass energy of 150 eV and a step size of 1 eV. The equipment was calibrated using C 1s (284.5 eV). High-resolution spectra were recorded in the binding energy regions for oxygen O 1s, titanium Ti 2p, carbon C 1s and nickel Ni 2p using a pass energy of 20 eV, 25 scans and step size of 0.1 eV. X-ray diffractometer (Bruker D2 Phaser 2nd generation) using CuKa radiation and a LynxEye XE-T detector was used to analyse the phase composition of the samples.

1.7. Electrochemical measurements

Before electrochemical measurements, the electrolyte was deaerated by an argon flow for 30 min, while during the measurements; the argon flow was maintained above the electrolyte. The three-electrode cell was composed of a working electrode containing the prepared catalysts, a counter electrode (Pt mesh or glassy carbon rod) and a reference electrode (Ag/AgCl/0.1 M KCl) and PGSTAT302N potentiostat/galvanostat (Metrohm Autolab) was used to conduct the tests. For comparison, electrochemical measurements were also performed using benchmark electrocatalysts, i.e., iridium oxide (IrO_2) for OER and 20% platinum on carbon (20% Pt/C) for HER, as working electrodes. All measurements were performed in 1 M NaOH, and the applied potentials were converted to the reversible hydrogen electrode (RHE) by using the following equation:

$$E_{RHE} = E_{Ag/AgCl} + 0.059\ pH + 0.197\ V \quad (1)$$

The overpotential (η) was calculated according to the following formula:

$\eta_{HER} = |E_{RHE}|$ (2), for hydrogen evolution reaction (HER)

and $\eta_{OER} = |E_{RHE} - 1.23V|$ (3) for oxygen evolution reaction (OER).

First, five CV cycles, were recorded in the potential range of −1.0 - +1.0 V vs. Ag/AgCl/ 0.1 M KCl at a scan rate of 50 mV s^{-1}. The HER and OER activities and stabilities were verified by linear scan voltammetry (LSV) and chronopotentiometry (CP). LSV were measured with the rate of 10 mV s^{-1}. Tafel plots were obtained by plotting η_{HER} or η_{OER} against log (j) from their corresponding LSV data, where j is the current density given in mA cm^{-2}. In order to test stability, chronopotentiometric measurements were carried out for 24 h. During the measurements, the current density was increased every 6 h in a staircase pattern: 10, 20, 50, and 100 mA cm^{-2} for OER and -10, -20, -50, and -100 mA cm^{-2} for HER. The electrochemical impedance spectroscopy (EIS) data were recorded within the frequency range from 20 kHz to 0.1 Hz with 10 mV amplitude of the AC signal. The applied DC potential to the working electrode was 0 V. The EIS data was fitted with the electric equivalent circuit (EEC) using

an EIS Spectrum Analyser program [5]. The modified Powell algorithm was used with amplitude weighting r_a:

$$r_a(\omega,P_1...P_M) = \frac{r_c^2}{N-M} \quad (4)$$

where N is the number of points, M is the number of parameters, ω is the angular frequency, $P_1...P_M$ are parameters. Parameter r_c is defined as:

$$r_c^2 = \sum_{i=1}^{N} \frac{(Z_i^{'} - Z_{i_{calc}}^{'})^2 + (Z_i^{''} - Z_{i_{calc}}^{''})^2}{Z_i^{'2} + Z_{i_{calc}}^{''\ 2}} \quad (5)$$

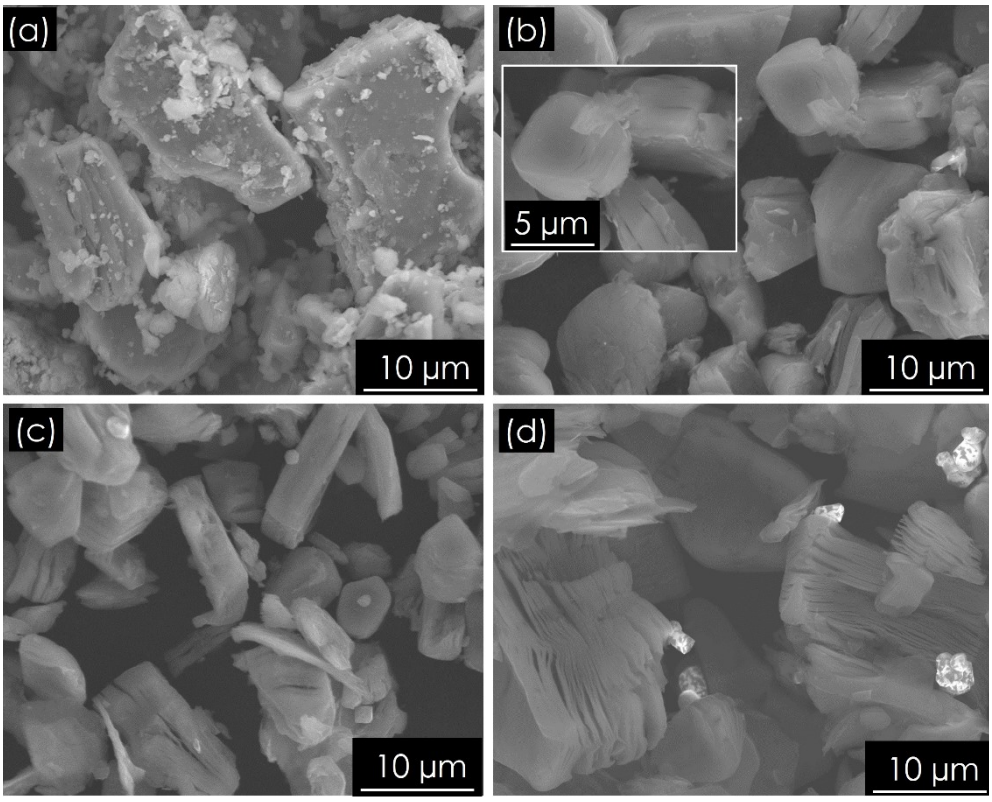

Figure S3. (a) SEM images of Ti_3AlC_2 MAX phase**.** SEM images of fabricated MXenes according to the electrochemical method (b) MX-100, (c) MX-200 (inset: high resolution SEM image of MXenes flakes), and the traditional one: (d) MX-HF.

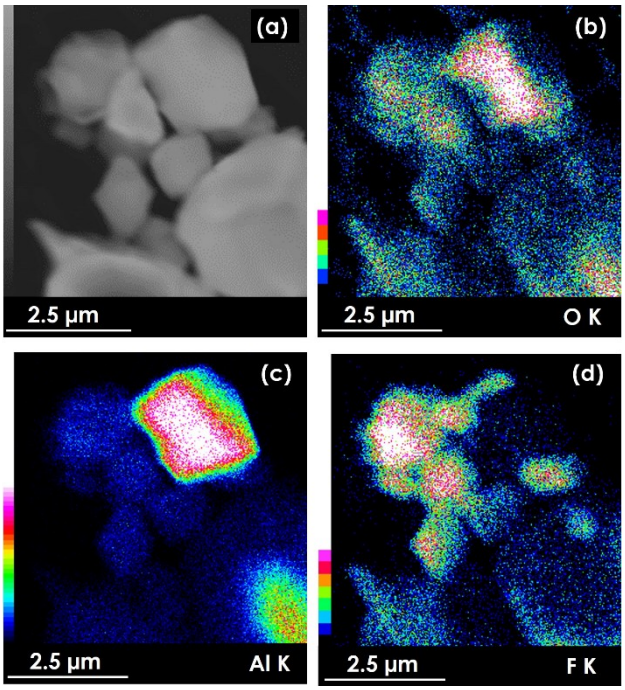

Figure S4. (a) TEM image and (b)-(d) distribution mapping recorded for (b) O, (c) Al and (d) F of MX-300.

Table S1. Peak positions and corresponding vibrational modes for MXene based materials

Peak position	**Corresponding vibrational mode**
120 cm^{-1}	resonance peak of MXenes
206 cm^{-1}	out-of-plane A1g (Ti, C, O)
361 cm^{-1}	in-plane Eg (Ti, C, O)
736 cm^{-1}	out-of-plane A1g (Ti, C, O)

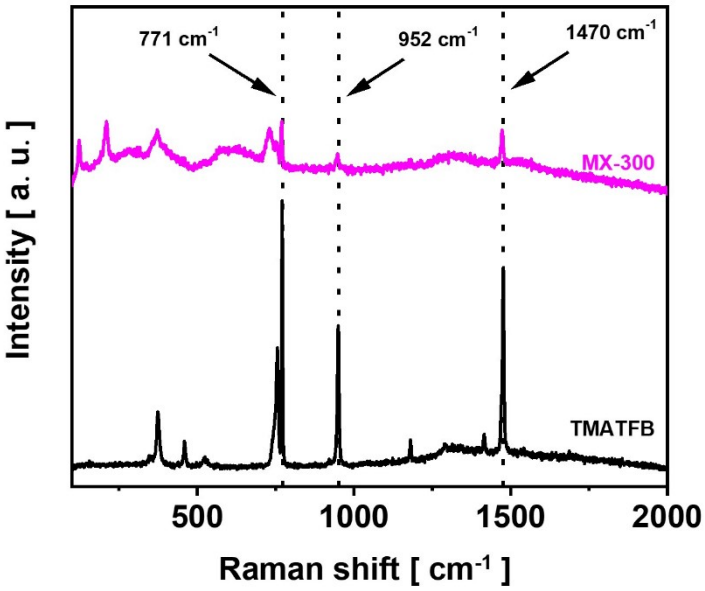

Figure S5. Raman spectra of TMATFB and MX-300.

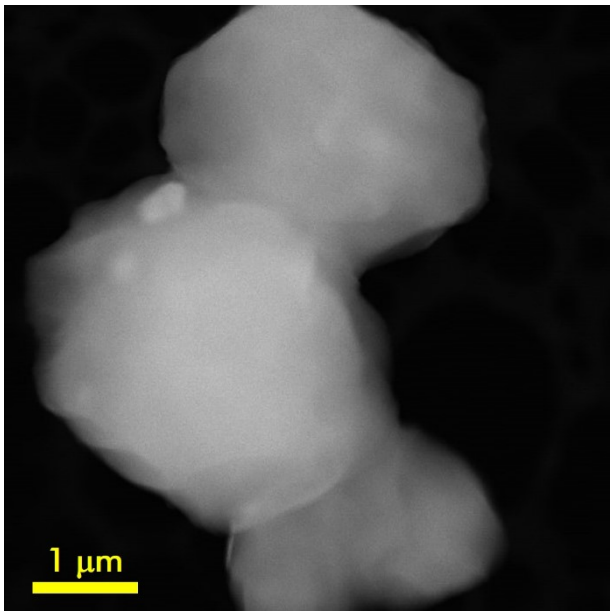

Figure S6. High-resolution TEM images of MX-300.

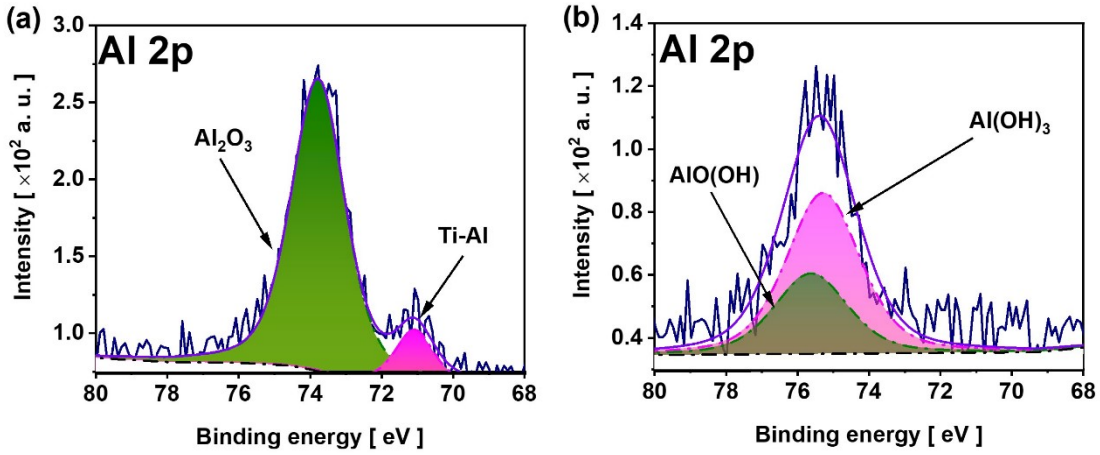

Figure S7. High-resolution XPS spectra of Al 2p for (a) Ti_3AlC_2 MAX phase, and (b) MX-300.

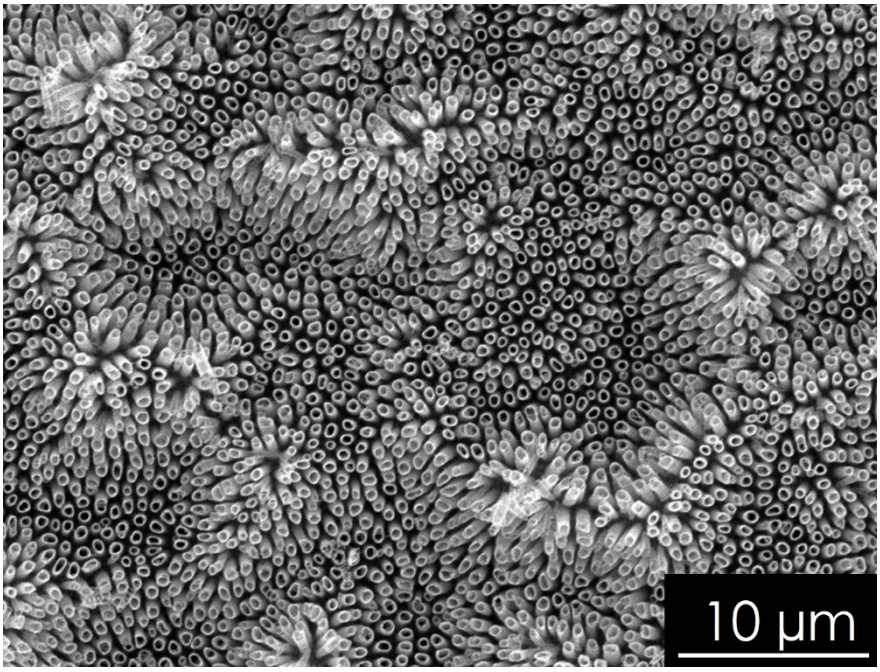

Figure S8. SEM image of anodic titania nanotubes TN.

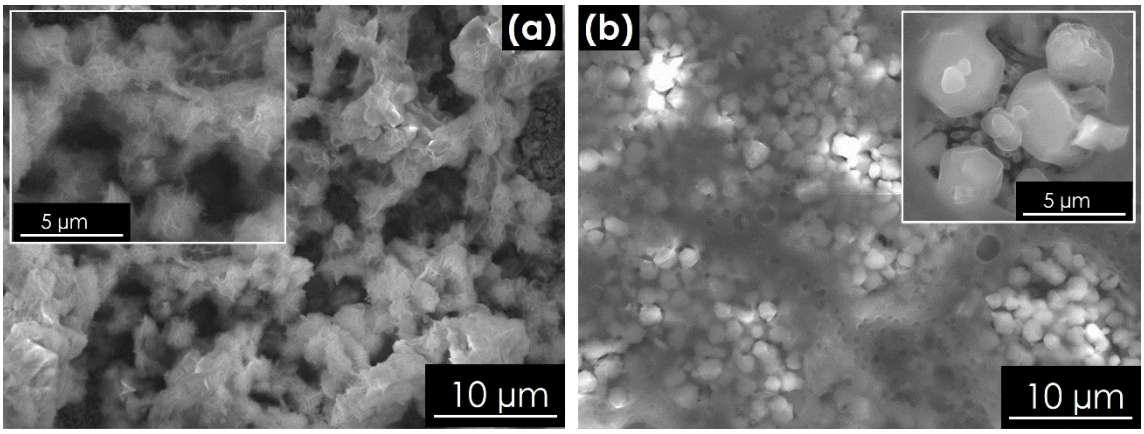

Figure S9. SEM images of NiMX-300 deposited onto TN annealed in: (a) air (inset: corresponding high resolution image), and (b) in hydrogen atmosphere (inset: corresponding high resolution image).

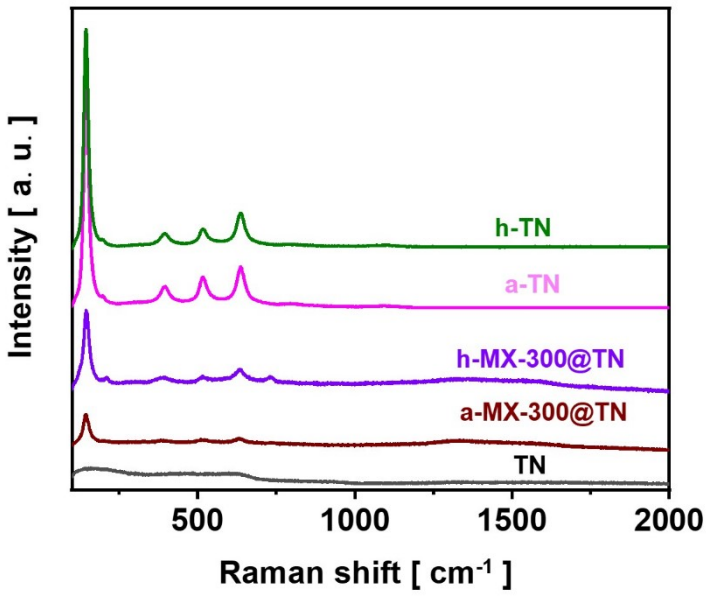

Figure S10. Raman spectra of as-anodized titania nanotubes (i.e., TN), annealed nanotubes (i.e., in air a-TN and under hydrogen atmosphere h-TN), and modified with MXenes and annealed in air and hydrogen atmosphere, respectively: a-MX-300@TN and h-MX-300@TN.

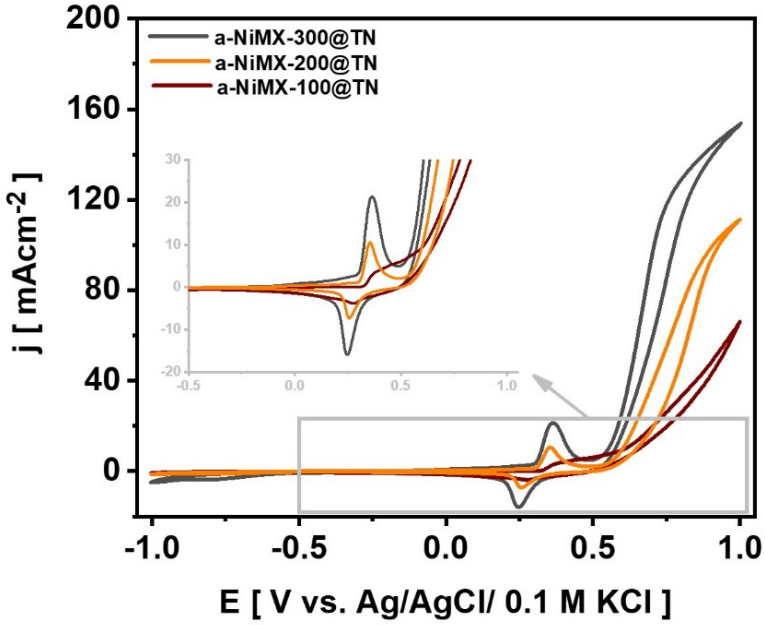

Figure S11. Cyclic voltammetry of the a-NiMX-100@TN, aNiMX-200@TN and NiMX-300@TN samples atmosphere recorded at the scan rate of 50 mV s^{-1} in 1 M NaOH.

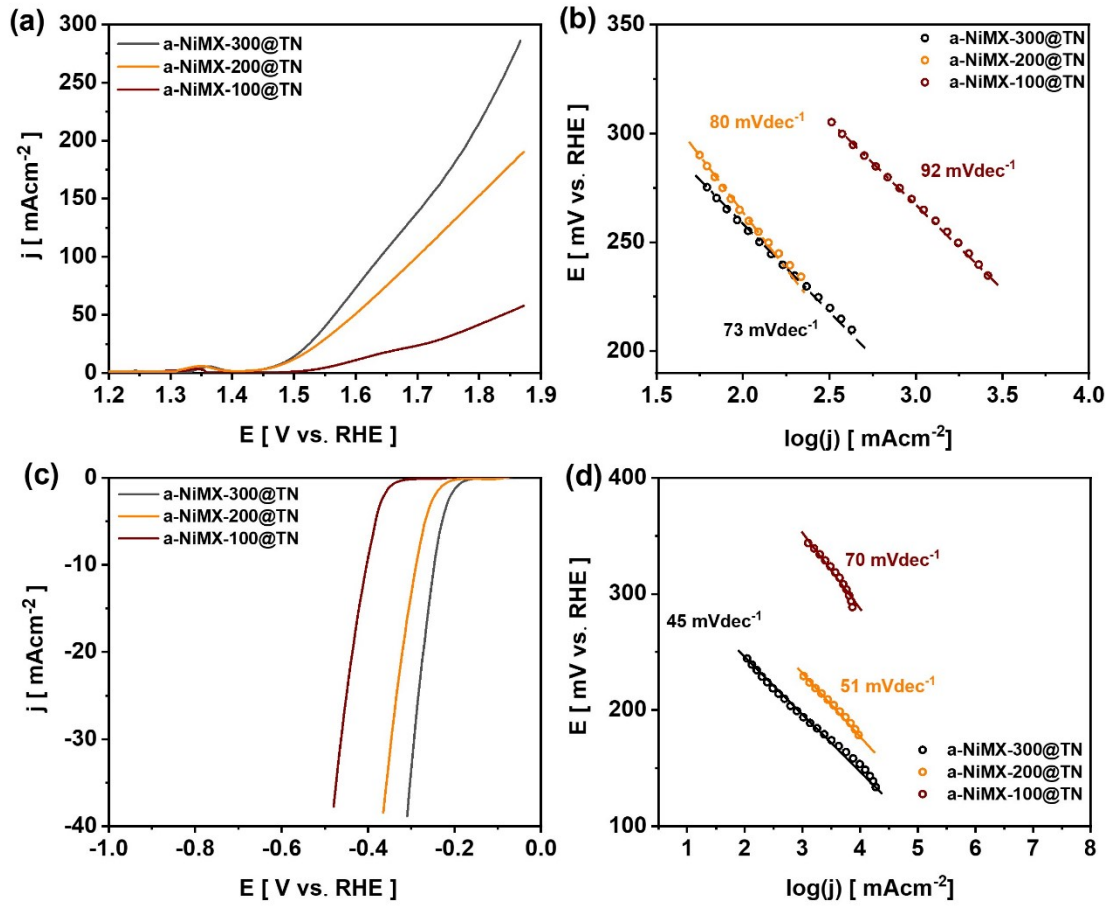

Figure S12. (a) Linear voltammetry polarization curves of a-NiMX-100@TN, aNiMX-200@TN and NiMX-300@TN catalysts, tested for the OER in 1 M NaOH, at the rate of 10

mV s^{-1}. (b) Tafel plots corresponding to LV in (a). (c) Linear voltammetry polarization curves of a-NiMX-100@TN, aNiMX-200@TN and NiMX-300@TN catalysts, tested for the HER in 1 M NaOH, at the rate of 10 mV s^{-1}. (b) Tafel plots corresponding to LV in (c).

Table S2. OER performances of electrocatalysts based on MXenes modified with Ni.

Electrocatalyst	Tafel slope / $mVdec^{-1}$	Overpotential at 10 mA cm^{-2} / mV	Electrolyte	Reference
β-NiS@$Ni(OH)_2$	53	330	1 M KOH	[6]
Ni/$Ni(OH)_2$	70	270	1M KOH	[7]
NiFe/Ti_3C_2Tx	55.1	334	1 M KOH	[8]
NiMoSe/Ti_3C_2Tx@CC	189	320	1 M KOH	[9]
NiFe-P/Ti_3C_2Tx	72.3	290	1 M KOH	[10]
NiCu/ Ti_3C_2Tx –NF	146	185	0.1 M KOH	[11]
$NiFe_2O_4$/Ti_3C_2	73.6	266	1 M KOH	[12]
$Ni_{0.9}Fe_{0.1}PS_3$@ Ti_3C_2Tx	36.5	282	1 M KOH	[13]
a-NiMX-300@TN	73	260	1 M NaOH	This work

Table S3. HER performances of electrocatalysts based on MXenes modified with Ni.

Electrocatalyst	Tafel slope / $mVdec^{-1}$	Overpotential at 10 mA cm^{-2} / mV	Electrolyte	Reference
Ni/$Ni(OH)_2$	53	77	1M KOH	[7]
Ni-MOF/Ti_3C_2Tx	56.15	181	0.1 M NaOH	[14]
NiMoSe/Ti_3C_2Tx@CC	45	203	1 M KOH	[9]
NiFe-P/Ti_3C_2Tx	112	173	1 M KOH	[10]
NiCu/ Ti_3C_2Tx-NF	104	111	0.1M KOH	[11]
Ti_3C_2Tx/Ni_3S_2-NF	45	72	1 M KOH	[15]
Ni- Ti_3C_2Tx	124	109	1 M KOH	[16]
NiMn/Ti_3C_2Tx	220	460	1 M NaOH	[17]
a-NiMX-300@TN	45	247	1 M NaOH	This work

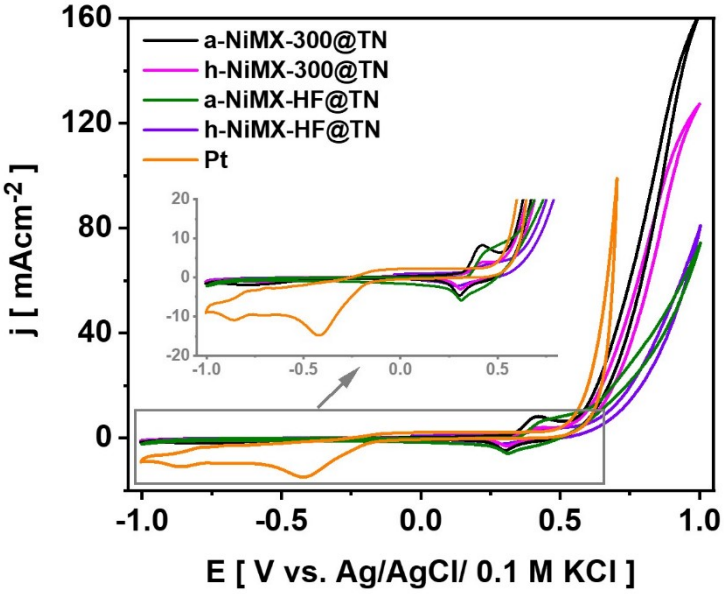

Figure S13. (a) Cyclic voltammetry of the NiMX-300@TN and NiMX-HF@TN samples annealed in air and under hydrogen atmosphere and Pt disc electrode recorded at the scan rate of 50 mV s^{-1} in 1 M NaOH.

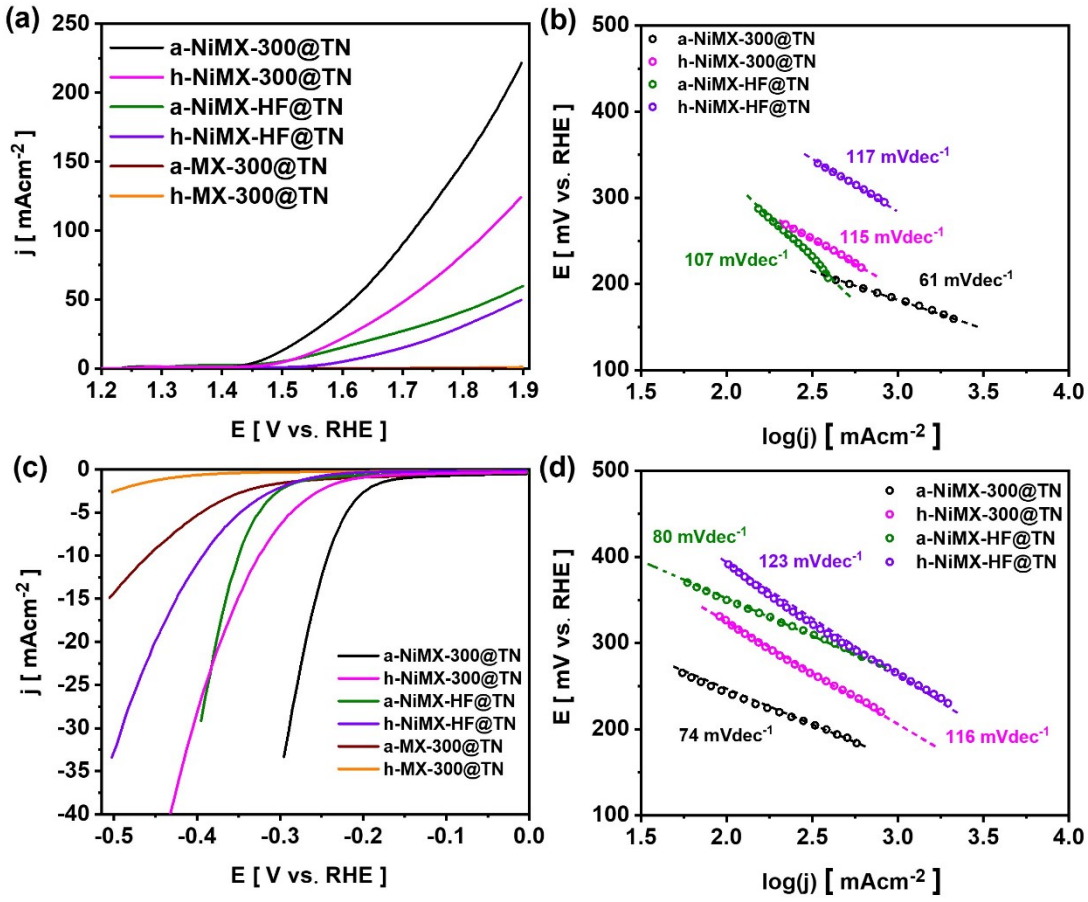

Figure S14. (a) Linear voltammetry polarization curves of a-NiMX-300@TN, h-NiMX-300@TN, a-NiMX-HF@TN, h-NiMX-HF@TN, a-MX-300@TN and h-MX-300@TN

catalysts, tested for the OER in 1 M NaOH, at the rate of 10 mV s^{-1}. (b) Tafel plots correponsifn to LV in (a). (c) Linear voltammetry polarization curves of of a-NiMX-300@TN, h-NiMX-300@TN, a-NiMX-HF@TN, h-NiMX-HF@TN, a-MX-300@TN and h-MX-300@TN catalysts, tested for HER in 1 M NaOH, at the rate of 10 mV s^{-1}. (b) Tafel plots corresponding to LV in (c).

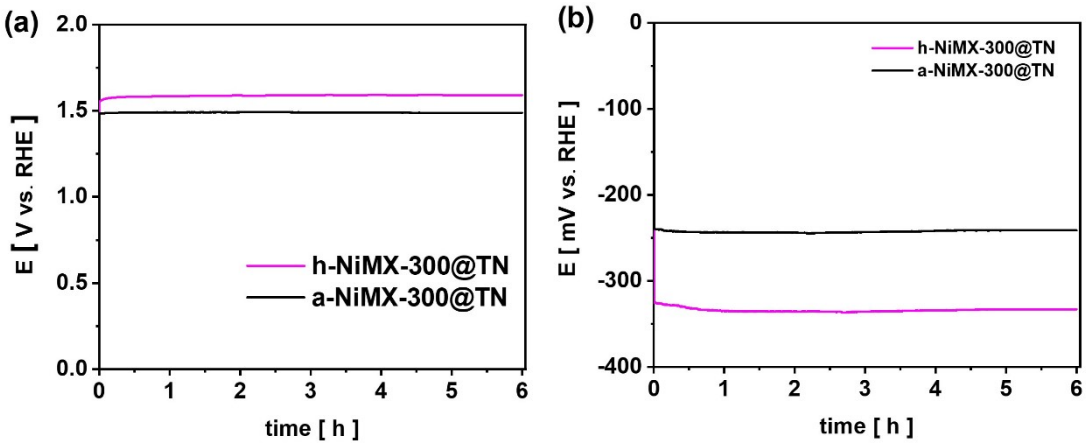

Figure S15. The chronopotentiometric curves of h-NiMX-300@TN and a-NiMX-300@TN over 6 hours were recorded under galvanostatic conditions (a) at 10 mA cm^{-2} and (b) at -10 mA cm^{-2}.

Table S4. The set of the values of overpotential and Tafel slope of a-NiMX-300@TN, h-NiMX-300@TN, a-NiMX-HF@TN and h-NiMX-HF@TN samples.

Catalyst	Type of the counter electrode	OER		HER	
		Tafel slope / $mVdec^{-1}$	Overpotential at 10 mA cm^{-2} / mV	Tafel slope / $mVdec^{-1}$	Overpotential at 10 mA cm^{-2} / mV
a-NiMX-300@TN	glassy carbon rod	73	260	45	247
	Pt mesh e	61	255	74	239
h-NiMX-300@TN	glassy carbon rod	77	280	67	322
	Pt mesh	115	360	116	327
a-NiMX-HF@TN	glassy carbon rod	110	370	108	346
	Pt mesh	115	340	80	350
h-NiMX-HF@TN	glassy carbon rod	135	460	150	398
	Pt mesh	117	440	123	392

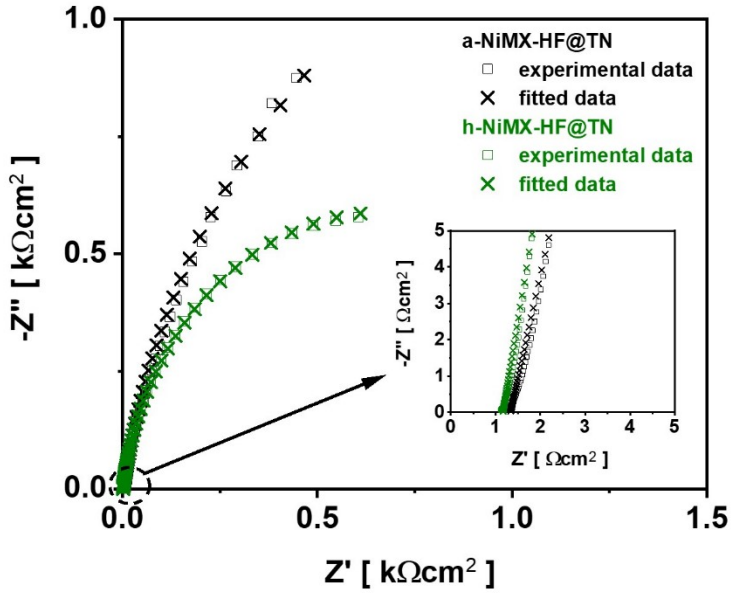

Figure S16. Nyquist representation of EIS spectra of h-NiMX-HF@TN and a-NiMX-HF@TN recorded at OCP in 1 M NaOH.

Table S5. Values of fitting parameters and calculated double-layer capacitance (C_{dl}) of the synthesized electrodes.

Sample	R_s (Ωcm^2)	R_{ct} ($k\Omega cm^2$)	Q_{in} ($k\Omega^{-1}cm^{-2}\ s^n$)	n	C_{dl} ($mFcm^{-2}$)
a-NiMX-300@TN	1	0.9	2.9	0.87	3.3
h-NiMX-300@TN	1	0.8	2.6	0.88	2.9
a-NiMX-HF@TN	1.1	1.3	0.9	0.87	1.2
h-NiMX-HF@TN	1.3	3.2	0.85	0.91	0.9

References

1 D.-S. Kouao, K. Grochowska, V. Stranak, P. Sezemsky, J. Gumieniak, A. Kramek, J. Karczewski, E. Coy, J. Hanus, O. Kylian, M. Sawczak and K. Siuzdak, *ACS Nano*, 2024, **18**, 10165–10183.

2 J. Huang, M. Feng, Y. Peng, C. Huang, X. Yue and S. Huang, *Small*, 2023, **19**, 2206098.

3 J. Wawrzyniak, K. Grochowska, J. Karczewski, P. Kupracz, J. Ryl, A. Dołęga and K. Siuzdak, *Surface and Coatings Technology*, 2020, **389**, 125628.

4 P. Rudzińska, J. Wawrzyniak, K. Grochowska, J. Karczewski, J. Ryl and K. Siuzdak, *Materials Science and Engineering: B*, 2023, **290**, 116324.

5 A. S. Bondarenko and G. A. Ragoisha, *J Solid State Electrochem*, 2005, **9**, 845–849.

6 B. Jansi Rani, N. Dhivya, G. Ravi, S. S. Zance, R. Yuvakkumar and S. I. Hong, *ACS Omega*, 2019, **4**, 10302–10310.

7 L. Dai, Z. Chen, L. Li, P. Yin, Z. Liu and H. Zhang, *Advanced Materials*, 2020, **32**, 1906915.

8 Y. Sun, Z. Wang, Q. Zhou, X. Li, D. Zhao, B. Ding and S. Wang, *Heliyon*, 2024, **10**, e30966.

9 M. Saquib, N. Srivastava, P. Arora and A. C. Bhosale, *International Journal of Hydrogen Energy*, 2024, **59**, 1132–1142.

10 L. Tan, J. Wang, S. Zhou, H. Zhu, J. Guo, Y. Chen, X. Li, Z. Dong, Q. Zhang and Y. Cong, *Journal of Colloid and Interface Science*, 2025, **689**, 137263.

11 A. Raveendran, M. Chandran, M. R. Siddiqui, S. M. Wabaidur, S. Angaiah and R. Dhanusuraman, *Sustainable Energy Fuels*, 2024, **8**, 1509–1525.

12 P. V. Shinde, P. Mane, B. Chakraborty and C. Sekhar Rout, *Journal of Colloid and Interface Science*, 2021, **602**, 232–241.

13 C. Du, K. N. Dinh, Q. Liang, Y. Zheng, Y. Luo, J. Zhang and Q. Yan, *Advanced Energy Materials*, 2018, **8**, 1801127.

14 K. Gothandapani, G. Tamil Selvi, R. Sofia Jennifer, V. Velmurugan, S. Pandiaraj, M. Muthuramamoorthy, S. Pitchaimuthu, V. Raghavan, A. C. Josephine Malathi, A. Alodhayb and A. Nirmala Grace, *International Journal of Hydrogen Energy*, 2024, **52**, 1164–1171.

15 L. Tie, N. Li, C. Yu, Y. Liu, S. Yang, H. Chen, S. Dong, J. Sun, S. Dou and J. Sun, *ACS Appl. Energy Mater.*, 2019, **2**, 6931–6938.

16 S. M. Z. Mehdi, H. Ghulam Abbas, M. Ali, S. B. H. Rizvi, S. R. Choi, J. C. Goak, Y. Seo, S. Kumar and N. Lee, *Energy & Environ Materials*, 2025, e12876.

17 S. Goudarzi and A. Ghaffarinejad, *Materials Today Sustainability*, 2025, **30**, 101109.